Optimized detection of normal vibration modes of atomic force microscope cantilevers with the optical beam deflection method

Tilman E. Schäffer[a] and Harald Fuchs
Center for Nanotechnology (CeNTech) and Physikalisches Institut, Westfälische Wilhelms-Universität Münster, Gievenbecker Weg 11, 48149 Münster, Germany

(Received 13 October 2004; accepted 17 January 2005; published online 6 April 2005)

Recently, higher-order normal vibration modes of atomic force microscope cantilevers were utilized for functional imaging applications. Here, we present a detailed theoretical investigation of the sensitivities with which these modes are detected using the optical beam deflection method. The detection sensitivities depend strongly on the size and position of the focused optical spot. Optimization of the sensitivities is performed for the individual (transverse) normal modes. For the case that multiple normal modes need to be detected simultaneously, a universal sensitivity function is constructed. This function generates accurate values for the detection sensitivity as a function of spot diameter and mode number. Finally, different optimization strategies for the simultaneous detection of multiple normal modes are presented. © *2005 American Institute of Physics*. [DOI: 10.1063/1.1872202]

I. INTRODUCTION

Since the invention of the atomic force microscope[1] (AFM), both static and dynamic modes have been used for the measurement of sample properties in various environmental conditions. Prominent examples for imaging modes are the contact mode,[1] the tapping mode,[2,3] and noncontact modes.[4–6] Force spectroscopic measurements can be performed either statically[7,8] or dynamically.[9–12]

The dynamic imaging and spectroscopy methods traditionally utilize the first normal (fundamental) vibration mode of the cantilever. It has been shown, however, that higher-order normal modes can be also used for functional imaging of surfaces. Minne *et al.*[13] have measured surface elasticity by driving a cantilever that was partially coated with zinc oxide at the second normal mode. In atomic force acoustic microscopy,[14,15] ultrasonic sample surface vibrations in the megahertz range are coupled to the AFM cantilever. The resulting cantilever dynamics can be modeled only if higher-order normal modes are included.[16] Likewise, higher-order normal modes underlie the "forest of peaks" frequency spectrum obtained in tapping mode in liquid.[17] Higher-order normal modes were used to obtain material contrast on heterogeneous surfaces.[18,19] Furthermore, it has been shown that a quantitative description of tapping mode AFM is possible only if the simultaneous excitation of higher-order normal modes is considered.[20] It is thereby possible to reconstruct the time course of the tip-sample force.[21] The feasibility for spatially resolved force spectroscopy by the simultaneous excitation of multiple normal modes has been proposed.[22]

For a quantitative interpretation of the measurement results, the amplitudes of the normal vibration modes need to be accurately determined. The most widespread method for detecting the deflection of an AFM cantilever is the optical beam deflection method.[23,24] In this method, an optical beam is focused to a spot on the cantilever and reflected from it onto a position-sensitive photodetector, whereby angular deflections of the cantilever are detected. A theoretical formalism for the sensitivity with which cantilever deflections are detected was developed based on optical diffraction theory.[25,26] Using this formalism, the thermal noise in the AFM was calculated using a modal decomposition,[27] corrections in thermal spring constant calibration due to a finite size and position of the focused spot were derived.[28] This formalism was also used to show that there can be (almost) pole-zero cancellations that lead to a significantly reduced detection sensitivity for higher-order modes.[29]

Here, we present a detailed quantitative analysis of the sensitivities with which the normal modes are detected using the optical beam deflection method. First, the formalism for the optical detection sensitivity is extended to a more general case. Second, the functional description of the normal modes is reviewed and approximations are given. Third, the detection sensitivities as a function of diameter and position of the focused spot for different normal modes are calculated and discussed. Fourth, optimization of the detection sensitivities for the individual normal modes is performed. Fifth, simultaneous detection of multiple normal modes is discussed. Finally, different optimization strategies for the simultaneous detection of multiple normal modes are presented. In all cases, quantitative results are given.

II. THEORY

A. Optical detection sensitivity

The sensitivity of the optical beam deflection method was derived using classical diffraction theory for the special case when the axis of the incident optical beam and the axis of the z scanner are perpendicular to the cantilever plane.[25,26] Here, we derive the more general case for an arbitrary angular orientation of the incident beam, the scanner, and the cantilever, respectively. For this purpose, we consider three

[a]FAX: +49 (251) 833-3602; electronic mail: tilman.schaeffer@uni-muenster.de

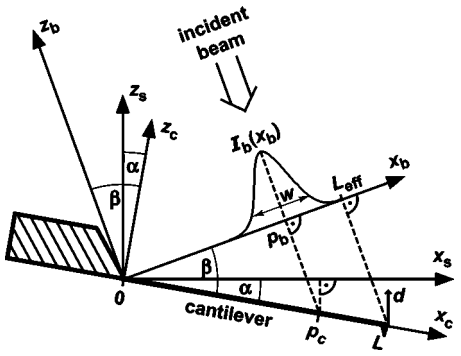

FIG. 1. Schematic of the optical beam deflection setup. The incident beam, the scanner, and the cantilever are arbitrarily tilted with respect to each other (with angles α and β). Three different reference frames are therefore considered: That of the incident beam (x_b, z_b), that of the scanner (x_s, z_s), and that of the cantilever (x_c, z_c). The incident beam has a Gaussian irradiance profile in its focus, $I_b(x_b)$, with a $1/e^2$ focused spot diameter w and center position p_b (both along x_b). Note that the focused spot is typically elliptical in shape, and that only the spot diameter along x_b is relevant for the optical deflection sensitivity—the spot diameter along the cantilever width (perpendicular to the paper plane) is arbitrary as long as no light power is spilled over the lateral cantilever edges. Viewed in the direction of the incident beam, the cantilever appears shortened with an effective length L_{eff}.

different coordinate reference frames (Fig. 1): (1) that of the incident beam with coordinates (x_b, z_b), (2) that of the scanner with coordinates (x_s, z_s), and (3) that of the cantilever with coordinates (x_c, z_c). The axis of the incident beam is parallel to the z_b axis, the axis of the z scanner is parallel to the z_s axis, and the undeflected cantilever is along the x_c axis.

The incident optical beam in an AFM is usually emitted from a laser diode. Its shape is highly elliptical (aspect ratio 1:2–1:3) and approximately Gaussian. This beam is focused to an elliptical spot on the cantilever, and is oriented such that the main axes of the spot are along the cantilever length and along the cantilever width, respectively. Well within the depth of focus of the incident beam, $|z_b| \ll \pi w^2/(4\lambda)$, the one-dimensional irradiance distribution along x_b can be written as

$$I(x_b) = \sqrt{\frac{8}{\pi}} \frac{P_0}{w} e^{-2[2(x_b - p_b)/w]^2}, \tag{1}$$

where w is the diameter of the focused spot at the $1/e^2$-irradiance points along x_b, p_b is the position of the focused spot on the x_b axis, and P_0 and λ are the total power and wavelength of the incident beam, respectively. In Eq. (1), the positional variable along the direction perpendicular to both x_b and z_b (i.e., along the cantilever width) was integrated out. We note that the spot diameter along the cantilever width is arbitrary as long as no significant light power is spilled over the lateral edges of the cantilever, i.e., as long as the spot diameter along the cantilever width is somewhat smaller than the cantilever width.[25] This condition is often automatically satisfied when considering the large aspect ratio of the beam from the laser diode. When even larger aspect ratios are required, additional cylindrical focusing optics or an adjustable aperture[25] might be necessary. A slight spill of light power over the lateral cantilever edges, however, does not significantly alter the results of this paper. For the diffraction calculations, we consider the effective length of the cantilever as viewed in the direction of the incident beam (along z_b),

$$L_{\text{eff}} = L \cos \beta. \tag{2}$$

We also consider the effective deflection of the cantilever tip, d_{eff}, as viewed in the direction of the incident beam. When the z scanner deflects the cantilever by d (along z_s), then the actual cantilever deflection (along z_c) is $d/\cos\alpha$. In the direction of the incident beam, this appears as

$$d_{\text{eff}} = d \frac{\cos \beta}{\cos \alpha}. \tag{3}$$

In most AFMs, a split photodiode is used as a detector, delivering as detection signal the difference in incident power on each segment: $P_A - P_B$. We define the optical detection sensitivity for such a detector as the detection signal per unit tip deflection in the direction of the z scanner. By using Eq. (10) of Ref. 25 and substituting L_{eff} and d_{eff} for L and z, respectively, we extend this equation to be valid for a setup with arbitrary angular orientations of cantilever, scanner, and incident beam, respectively. The optical detection sensitivity can therefore be written as

$$\sigma_n(w, p_b) = \sigma_0 \frac{w}{L_{\text{eff}}} f_n\left(\frac{w}{L_{\text{eff}}}, \frac{p_b}{L_{\text{eff}}}\right). \tag{4}$$

Equation (4) is the product of a prefactor,

$$\sigma_0 = \sqrt{\frac{\pi}{2}} \frac{4 P_0 \cos \beta}{\lambda \cos \alpha}, \tag{5}$$

a factor, w/L_{eff}, that is proportional to the focused spot diameter and a factor that depends on the functional shape of the vibrating cantilever,

$$f_n(u, v) = \frac{4}{\pi u^2} \int_0^1 dq \int_0^1 dq' \frac{h_n(q) - h_n(q')}{q - q'} \times \exp\left[\frac{-4(q - v)^2 - 4(q' - v)^2}{u^2}\right]. \tag{6}$$

$h_n(q)$ is the normalized shape of the cantilever (see below). $f_n(u, v)$ can be thought of as the "effective slope" of the section of the cantilever that is probed by the focused spot. It is this effective slope what is really measured by the optical beam deflection method. In the case that non-Gaussian focused spots are used, the formulas need to be adjusted appropriately.[25]

In the case that a relative detection signal is used, $(P_A - P_B)/(P_A + P_A)$, σ_0 needs to be divided by the total power of the reflected light, $P_{\text{det}} = P_A + P_B = \int_0^{L_{\text{eff}}} I(x)\, dx$. The requirements for Eqs. (4)–(6) to be valid are (a) the width of the focused spot (perpendicular to both x_b and z_b) is smaller than the width of the cantilever so that no significant light power is spilled over the lateral edges of the cantilever (as discussed in the previous paragraph), (b) the cantilever deflection is small compared to its length:[25] $|z_{\text{eff}}| \ll L_{\text{eff}}$, and (c) the length of the projection of the cantilever onto the z_b axis is much smaller than the depth of focus: $L \sin(\beta) \ll \pi w^2/(4\lambda)$. In most of the cases considered here, $P_{\text{det}} = \text{const}$, therefore op-

timizing the sensitivity is approximately equivalent to optimizing the signal-to-noise ratio (in the case of fundamentally limiting shot noise).

B. Functional shape of normal vibration modes

The functional shapes of the normal modes of free, undamped, transverse vibrations of a rectangular cantilever are given by[30]

$$h_n(q) = \frac{(-1)^n}{2}\left[\cos \kappa_n q - \cosh \kappa_n q - \frac{\cos \kappa_n + \cosh \kappa_n}{\sin \kappa_n + \sinh \kappa_n}(\sin \kappa_n q - \sinh \kappa_n q)\right]. \quad (7)$$

n denotes the mode number and $h_n(q)$ is normalized so that at the base ($q=0$), $h_n(0)=0$, and at the tip ($q=1$), $h_n(1)=1$. The dimensionless wave numbers, κ_n, are the solutions of the characteristic equation, $\cos \kappa_n \cosh \kappa_n = -1$, with discrete solutions $\kappa_n \cong 1.875,\ 4.694,\ 7.855,\ \pi(n-1/2)$ for $n=1,2,3,\geqslant 4$, respectively. To circumvent computational inaccuracies for large mode numbers rooted in the subtraction of similarly large terms in Eq. (7), we derived an approximation that is much easier to compute (by rewriting the hyperbolic functions in terms of exponentials and dropping small terms):

$$h_n(q) \cong \frac{(-1)^n}{2}\left[\sqrt{2}\sin\left(\kappa_n q + \frac{3\pi}{4}\right) - e^{-\kappa_n q}\right] + \frac{e^{-\kappa_n(1-q)}}{2}, \quad \text{for } n \gtrsim 4. \quad (8)$$

The functional shapes of the first five normal modes are shown in Fig. 2. Common to all modes is that their maximum deflection and their maximum slope are located at the tip, with $h_n'(1) \cong 1.377,\ 4.781,\ 7.849,\ \kappa_n$ for $n=1,2,3,\geqslant 4$, respectively. For the convenience of the following discussion, we define the wavelengths of the vibration modes, Λ_n, as they appear in the direction of the incident beam (i.e., in the projection onto the x_b axis):

$$\Lambda_n = \frac{2\pi}{\kappa_n} L_{\text{eff}}. \quad (9)$$

For large mode numbers, the mode wavelength equals two times the distance between two central vibration nodes as viewed in the direction of the incident beam.

III. RESULTS AND DISCUSSION

A. Optimization of the detection sensitivity

The absolute value of the optical detection sensitivity as a function of spot diameter and position (both along x_b) [Eq. (4)] is displayed as grayscale plot for the first five normal modes of a clamped-free rectangular cantilever [Figs. 3(a)–3(e)]. The brightness encodes the absolute value of the sensitivity, where larger values of the brightness correspond to larger absolute values of the sensitivity. It can be seen that the detection sensitivity strongly depends on those focused spot parameters (diameter and position) and on the functional shape of the cantilever (mode number n). To enhance the quantitative aspect of the plots, contour lines are introduced. The point in each grayscale plot where the sensitivity is globally optimized (from now on referred to as "globally optimized detection sensitivity") is marked with an "×." The point in each plot where the sensitivity is locally optimized and closest to the tip (from now on referred to as "tip-optimized detection sensitivity") is marked with a "+."

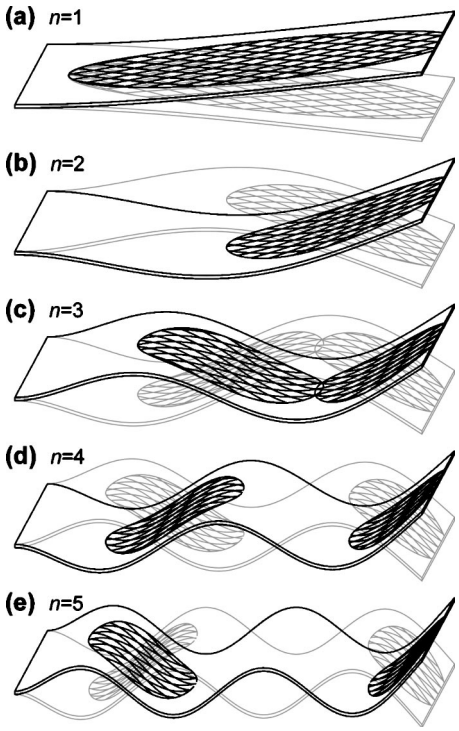

FIG. 2. Functional shapes of the first five normal vibration modes. The cantilever is clamped at its base (left side) and free at its tip (right side). The crosshatched areas outline the focused spots that "globally optimize" and "tip optimize" the detection sensitivity for each mode. For the first and second mode, these two spots are identical. For the third and higher modes, larger detection sensitivities are achieved for a spot close to the base (globally-optimized spot, left-hand side) than for a spot close to the tip (tip-optimized spot, right-hand side).

For the first normal mode [Fig. 3(a)], globally optimized and tip-optimized detection sensitivities coincide ($|\sigma_1/\sigma_0| \cong 0.783$) and are achieved when spot diameter and position are $w/L_{\text{eff}} \cong 0.952$ and $p_b/L_{\text{eff}} \cong 0.569$, respectively. In other words, optimum detection sensitivity for the first normal mode, which is the relevant mode in most ac-mode imaging and spectroscopy techniques, is obtained when the spot diameter is 95% of the effective cantilever length, and when the spot center is positioned at 57% on the distance from the cantilever base to the tip. The sensitivity decreases when the spot diameter and position deviate from those optimum values. This result refines a previous finding, where the detection sensitivity for a rigid, hinged cantilever was shown to be optimized when the spot diameter approximately equals the cantilever length and when the spot is positioned exactly at the center of the cantilever.[31,32] The outline of the optimum spot (area within the $1/e^2$-irradiance values) is shown on the cantilever [Fig. 2(a), crosshatched area]. Note that the size of the spot along the width of the cantilever is arbitrary as long as no light is spilled over the lateral edges of the cantilever.[25] For reference purposes, we note that the functional shape of a statically deflected cantilever, $h_{\text{static}}(p) = (3p^2 - p^3)/2$, such

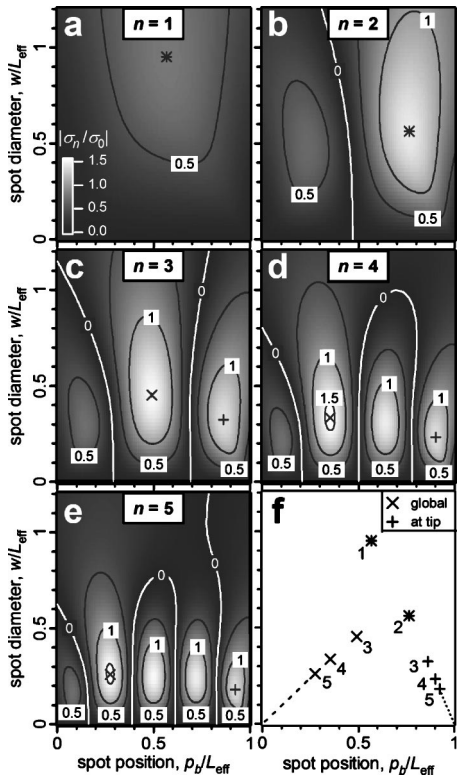

FIG. 3. (a)-(e) Optical beam detection sensitivity as a function of the focused spot diameter and position as combined grayscale/contour plot, for mode numbers $n=1$–5. Areas with a bright (dark) color correspond to large (small) absolute values of the detection sensitivity. The extremum with the largest absolute value of the sensitivity for each mode (globally optimized) is marked with an "×," the extremum closest to the tip (tip optimized) is marked with a "+." Contour lines with zero sensitivity are present for $n \geqslant 2$. (f) Globally-optimized and tip-optimized focused spot diameters and positions for the different normal modes. The dashed/dotted lines symbolize spot diameters and positions for mode numbers larger than 5.

as occurs during contact mode imaging or during force curves, is very similar to that of the first normal vibration mode. For such a statically deflected cantilever, optimum detection sensitivity ($|\sigma_{\text{static}}/\sigma_0| \cong 0.778$) is obtained when the spot diameter is 94% of the effective cantilever length, and when the spot center is positioned at 58% on the distance from the cantilever base to the tip.

For the second normal mode [Fig. 3(b)], globally optimized detection sensitivity ($|\sigma_2/\sigma_0| \cong 1.421$) is achieved when the spot diameter and position are $w/L_{\text{eff}} \cong 0.563$ and $P_b/L_{\text{eff}} \cong 0.763$, respectively. The outline of such a spot is shown on the cantilever [Fig. 2(b), crosshatched area]. There is a second local extremum of the sensitivity with a value of about half of the global maximum ($|\sigma_2/\sigma_0| \cong 0.685$), for a spot diameter and position of $w/L_{\text{eff}} \cong 0.474$ and $p_b/L_{\text{eff}} \cong 0.238$, respectively [Fig. 3(b)]. This local extremum of smaller value represents a focused spot that is distributed on the cantilever in the section closer to the base where the slope is of opposite sign.

For the third normal mode [Fig. 3(c)], globally optimized detection sensitivity ($|\sigma_3/\sigma_0| \cong 1.501$) is achieved when the spot diameter and position are $w/L_{\text{eff}} \cong 0.453$ and $p_b L_{\text{eff}} \cong 0.490$, respectively. This result is surprising at first, as there are two other local extrema, one closer to the tip and one close to the base. One might have expected that the sensitivity would be higher for the spot close to the tip (tip-optimized sensitivity), as the highest slope always occurs at the tip. An intuitive explanation for this result will now be given. There are two effects for spots with a finite size that affect the detection sensitivity [see Eq. (4)]: (1) The larger the spot diameter, the higher the absolute value of the detection sensitivity. (2) The larger the absolute value of the effective cantilever slope in the section over which the focused spot is distributed, the higher the absolute value of the detection sensitivity. In other words, high detection sensitivity is generally achieved when the focused spot is sized and positioned such that it spans a large section of the cantilever over which the slope is of constant sign and of high absolute value. For the third normal mode, it occurs that the advantage of a large spot diameter for the globally optimized extremum weighs more than the advantage of a large effective slope for the tip-optimized extremum. The outlines of the globally optimized spot and of the tip-optimized spot are displayed on the cantilever as the left and the right crosshatched areas, respectively [Fig. 2(c)].

For even higher normal modes ($n \geqslant 4$), this trend continues; the globally optimized sensitivity is always larger than the tip-optimized sensitivity [Figs. 3(d) and 3(e)]. Specifically, the globally optimized sensitivity is always ($n \geqslant 2$) the local extremum that is second closest to the base. The outlines of the globally optimized spot and the tip-optimized spot for the fourth and fifth normal modes, respectively, are shown as the crosshatched areas in Figs. 2(d) and 2(e).

Separating two adjacent maxima, there is always a contour line of zero sensitivity [Figs. 3(b)–3(e), white contour lines]. This is because neighboring extrema of the sensitivity are of alternating sign (representing sections of positive and negative cantilever slopes). For small spot diameters ($w \ll \Lambda_n$) the zero-contour lines are located at those spot positions, p_b, for which the cantilever slope is zero: $h_n'(p_b/L_{\text{eff}}) = 0$. For an increasing spot diameter, the contour lines initially point perpendicularly away from the p_b axis, until the spot diameter passes the value of the globally optimized sensitivity, after which some of the contour lines deviate from this perpendicular orientation. When spot parameters are chosen on a zero-contour line, there will be zero detection sensitivity for the respective mode. These cases should therefore be avoided when the detection sensitivity is to be optimized.

B. Globally optimized sensitivity

The absolute values of the globally optimized detection sensitivities and the corresponding spot diameters and positions are listed in Table I. The absolute value of the globally optimized detection sensitivity is by far the smallest for $n = 1$; it is only about half as large as those for the higher-order modes. The reason for this is that when going from the first to the second mode, the effective cantilever slope increases at a rate about twice as large as the rate with which the focused spot diameter decreases. For higher-order modes, these two rates are comparable, and the absolute value of the sensitivity asymptotically plateaus at $|\sigma_n/\sigma_0| \cong 1.557$ for $n \geqslant 5$. Such a plateau does not occur in a simple geometric-

TABLE I. Globally optimized and tip-optimized spot diameter, w, spot position, p_b, and absolute value of the detection sensitivity, $|\sigma_n|$, as well as the mode wavelength, Λ_n, as a function of the mode number, n. For $n \geqslant 5$, two lines corresponding to two equivalent expressions for spot diameter and position are displayed [Eqs. (10)–(13)]. The values for a statically deflected cantilever are also shown. Note that the optimized detection sensitivity for mode number 1 is only about half of those for higher mode numbers.

Mode number		Globally optimized			Tip optimized		
n	Λ_n/L_{eff}	w/L_{eff}	p_b/L_{eff}	$\lvert\sigma_n/\sigma_0\rvert$	w/L_{eff}	p_b/L_{eff}	$\lvert\sigma_n/\sigma_0\rvert$
(static)	⋯	-identical to tip optimized-			0.944	0.583	0.778
1	3.351	-identical to tip optimized-			0.952	0.569	0.783
2	1.339	-identical to tip optimized-			0.563	0.763	1.421
3	0.800	0.453	0.490	1.501	0.325	0.862	1.368
4	0.571	0.335	0.353	1.560	0.233	0.901	1.371
$\geqslant 5$	$2/(n-1/2)$	$1.17/(n-1/2)$	$1.24/(n-1/2)$	1.557	$0.814/(n-1/2)$	$1-0.345/(n-1/2)$	1.370
		$0.586(\Lambda_n/L_{\text{eff}})$	$0.618(\Lambda_n/L_{\text{eff}})$		$0.407(\Lambda_n/L_{\text{eff}})$	$1-0.173(\Lambda_n/L_{\text{eff}})$	

optics treatment, where the spot could be focused to a point at the tip of the cantilever where the slope is largest. In this case, the sensitivity would instead increase indefinitely for increasing mode numbers, since $h_n'(1) \to \infty$ for $n \to \infty$.[33] Based on these results, it is interesting to speculate that the first normal mode, which is predominantly used in current ac imaging and spectroscopic techniques, might not be the most advantageous with respect to sensitivity and resolution, as compared to the higher-order modes.

For large mode numbers, the optimum spot diameter is expected at about half the mode wavelength, Λ_n. This way, the spot can be distributed in the section between two antinodes, making the spot diameter as large as possible without significantly "sampling" cantilever slopes of opposite sign. The numerically accurate calculation yields that the optimum spot diameter is even slightly larger,

$$w^{(n,\text{global})} \cong 0.586\Lambda_n \cong \frac{1.17}{n-1/2}L_{\text{eff}}, \quad \text{for } n \geqslant 5. \tag{10}$$

Here we utilized Eq. (9) with the approximation for κ_n. The spot is consequently positioned near the vibration mode that is closest to the base (excluding the base, compare Fig. 2). The numerically accurate calculation yields for the optimum spot position,

$$p_b^{(n,\text{global})} \cong 0.618\Lambda_n \cong \frac{1.24}{n-1/2}L_{\text{eff}}, \quad \text{for } n \geqslant 5. \tag{11}$$

The spot diameter decreases monotonically for increasing mode numbers. In the limit of high mode numbers, the spot diameter approaches zero, and the spot position approaches the base of the cantilever [Fig. 3(f), dashed line].

C. Tip-optimized sensitivity

The absolute values of the tip-optimized detection sensitivities and the corresponding spot diameters and positions are also listed in Table I. The tip-optimized detection sensitivity is smallest for $n=1$ and asymptotically plateaus at $\sigma_n/\sigma_0 \cong 1.370$ for $n \geqslant 5$. Just as in the case of the globally optimized sensitivity, the tip-optimized sensitivity of the first normal mode is by far the smallest, whereas all higher-order modes are detected with about the same sensitivity (if the spot parameters are adjusted individually).

For large mode numbers, the optimum spot diameter is expected to be somewhat smaller than that for the globally optimized case above. The reason for this is that the tip is "free," and therefore the distance between the tip and the last antinode before the tip is smaller than the distance between two central antinodes, thereby also reducing the optimum spot diameter. The numerically accurate calculation yields for the optimum spot diameter,

$$w^{(n,\text{tip})} \cong 0.407\Lambda_n \cong \frac{0.814}{n-1/2}L_{\text{eff}}, \quad \text{for } n \geqslant 5. \tag{12}$$

The spot is positioned near the vibration node that is closest to the tip (compare Fig. 2). The numerically accurate calculation yields for the optimum spot position,

$$p_b^{(n,\text{tip})} \cong L_{\text{eff}} - 0.173\Lambda_n \cong \left(1 - \frac{0.345}{n-1/2}\right)L_{\text{eff}}, \quad \text{for } n \geqslant 5. \tag{13}$$

Again, the spot diameter decreases monotonically for increasing mode numbers. In the limit of large mode numbers, the spot diameter approaches zero, and the spot position approaches the tip of the cantilever [Fig. 3(f), dotted line]. In the limit of large mode numbers, the tip-optimized sensitivity is ≅88.0% of the globally optimized sensitivity.

D. Simultaneous detection of multiple normal modes

If multiple normal modes need to be detected simultaneously, spot parameters need to be chosen that are as far as possible away from all zero-contour lines for all respective modes (Fig. 3). While it might be possible to find such parameters, it is much more straightforward to sacrifice a small amount of sensitivity and to choose a spot close to the tip, especially if a large number of modes need to be detected simultaneously. For example, we consider the spot diameters, $w^{(N,\text{tip})}$, and positions, $p_b^{(N,\text{tip})}$, that tip optimize the detection sensitivity for $N=3$, $N=6$, $N=10$, and $N=20$, respectively: $w/L_{\text{eff}} \cong 0.33$, 0.15, 0.086, 0.042, and $p_b/L_{\text{eff}} \equiv 0.86$, 0.94,

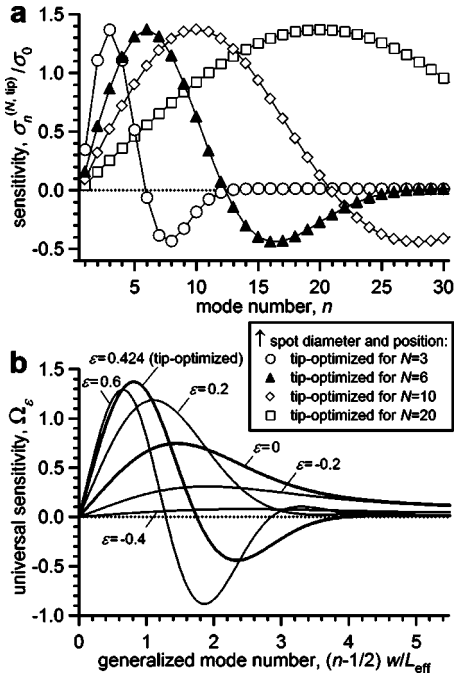

FIG. 4. (a) Detection sensitivity for different spot diameters and positions as a function of mode number, n. The sensitivity increases at first for increasing mode numbers, then exhibits a maximum, becomes negative, passes through a minimum, and asymptotically approaches zero. (The lines connect the markers to guide the eye.) (b) Universal sensitivity as a function of generalized mode number, $u=(n-1/2)w/L_{\text{eff}}$, for different values of $\varepsilon=(L_{\text{eff}}-p_b)/w$. From the universal sensitivity function, the detection sensitivities for given spot diameters, spot positions, and mode numbers can be looked up using Eq. (17).

0.96, 0.98, respectively. We plot the respective detection sensitivities, $\sigma_n^{(N,\text{tip})}:=\sigma_n(w^{(N,\text{tip})},p_b^{(N,\text{tip})})$, as a function of n [Fig. 4(a)]. There are a number of observations that can be made: (a) $\sigma_n^{(N,\text{tip})}$ increases monotonically from$n=1$–$n=N$. This is because the slope of the cantilever close to the tip increases for increasing mode numbers. (b) $\sigma_n^{(N,\text{tip})}$ is largest at $n=N$ (per definition). (c) For $n>N$, $\sigma_n^{(N,\text{tip})}$ decreases at first, passes through zero, and exhibits a minimum. (d) $\sigma_n^{(N,\text{tip})}\approx 0$ for $n\gtrsim 4N$. This is because the modal shapes for large mode numbers have a large number of alternating positive and negative slopes that average out the effective cantilever slope to zero.

E. Universal sensitivity function

Motivated by the similar functional shape of $\sigma_n^{(N,\text{tip})}$ for different N, we will now construct a universal sensitivity function that describes the optical detection sensitivities for all modes for a given spot diameter and position near the tip. First, we allow continuous spot diameters and positions while keeping their relationship as defined by

$$p_b = L_{\text{eff}} - \varepsilon w, \tag{14}$$

where ε denotes the distance of the spot position to the tip in multiples of the spot diameter. For example, $\varepsilon=0.424$ for the tip-optimized spot, as determined by Eqs. (12) and (13). Next, we note that now there are only two different length scales to consider: (1) the spot diameter, w, and (2) the mode wavelength, Λ_n [$\Lambda_n\cong 2L_{\text{eff}}/(n-1/2)$ for $n\geqslant 4$]. Identical detection sensitivities are generally obtained for identical ratios of spot diameter to mode wavelength [with Eq. (14) as condition]. Using this relationship, we construct a universal sensitivity function, $\Omega_\varepsilon(u)$, by defining in the limit of $w\to 0$ (i.e., $N\to\infty$) and for $n\gg 1$:

$$\Omega_\varepsilon(u) = \frac{1}{\sigma_0}\sigma_n\left(\frac{w}{L_{\text{eff}}}, 1-\varepsilon\frac{w}{L_{\text{eff}}}\right), \tag{15}$$

where u is the generalized mode number

$$u = \left(n-\frac{1}{2}\right)\frac{w}{L_{\text{eff}}}. \tag{16}$$

$\Omega_\varepsilon(u)$ is plotted in Fig. 4(b) for different values of the parameter ε. From $\Omega_\varepsilon(u)$, the detection sensitivity for a given spot diameter, spot position, and mode number can be found. It turns out that accurate results are obtained even for small mode numbers if simple (empirical) correction factors are introduced for $n=1$ and $n=2$: Given a spot of diameter w ($w/L_{\text{eff}}\leqslant 0.3$) that is positioned somewhere near the tip ($|\varepsilon|\lesssim 0.5$), the detection sensitivity for the nth mode, σ_n/σ_0, is obtained from the universal sensitivity function as

$$\frac{\sigma_n}{\sigma_0} \cong \Omega_\varepsilon\left[\left(n-\frac{1}{2}\right)\frac{w}{L_{\text{eff}}}\right]\begin{cases}0.876, & \text{if } n=1\\ 1.015, & \text{if } n=2\\ 1, & \text{if } n\geqslant 3.\end{cases} \tag{17}$$

The error of this approximation is $<1\%$. For higher mode numbers (and for smaller ε), the requirement on the spot size can be progressively relaxed (i.e., accurate results are also obtained for $w/L_{\text{eff}}\gtrsim 0.3$). For the first normal mode, alternative, simpler approximations can be found empirically: $\sigma_1/(\sigma_0 w/L_{\text{eff}})\cong 1.078$, 0.702, 0.344, 0.112 for $\varepsilon=0.424$, 0.2, 0, -0.2, respectively.

Important properties of $\Omega_\varepsilon(u)$ are [see Fig. 4(b)]: (a) the largest absolute value of $\Omega_\varepsilon(u)$ is located at $u\cong 0.184$ and $\varepsilon\equiv 0.424$ [$\Omega(0.814)\cong 1.370$]. This result is found also in Eqs. (12) and (13). Therefore, the universal sensitivity function is particularly important for $\varepsilon=0.424$ (tip-optimized spot), for which $\Omega_\varepsilon(u)$ has zeros at $u=1.75$ and $u=3.94$, and a minimum at $u=2.34$ [$\Omega_{0.424}(2.34)\cong -0.440$]. (b) $\Omega_\varepsilon(u)$ approaches zero for large u. When $\varepsilon\gtrsim 0.424$, $\Omega_\varepsilon(u)\approx 0$ for $u\gtrsim 4$. When $\varepsilon\lesssim 0.424$, $|\Omega_\varepsilon(u)|<0.1$ for $u\gtrsim 6.4$. (c) There are no zeros of $\Omega_\varepsilon(u>0)$ for $\varepsilon\lesssim 0.2$. This means that, in these cases, all modes are detected with the same (positive) sign of the sensitivity. (d) For large generalized mode numbers, $|\Omega_\varepsilon(u)|$ is largest for $\varepsilon\approx 0$. We use these properties for the discussion of optimization strategies in the following section.

F. Optimization strategies for the detection of multiple normal modes

In this section, we describe different strategies for optimizing the detection sensitivities of multiple normal modes. First, we assume that the diameter and position of the focused spot (along x_b) can be arbitrarily adjusted. (As discussed in Sec. II A, the diameter of the focused spot along the cantilever width is assumed to be smaller than the cantilever width.) The spot diameter can be adjusted, for example, by changing the diameter of the incident beam with an adjustable aperture in the incident-beam path.[25] Consider the

case that detection of all normal modes up to a given mode number, N, is required. (1) The most direct way (first strategy) is to choose a spot diameter and position that optimize the sensitivity for the Nth mode: $w/L_{\text{eff}} \cong 0.814/(N-1/2)$ and $\varepsilon \cong 0.424$. In this case, the sensitivity increases monotonically from mode number 1 to N (see Sec. IV D). (2) If it is not required that the sensitivity is largest for mode number N, the spot diameter and position could be chosen such that the sensitivity of the $(N+1)^{\text{th}}$ mode is zero: $w/L_{\text{eff}} \cong 1.75/(N+1/2)$ and $\varepsilon \cong 0.424$. The sensitivity then increases from mode number $n=1$ to the largest possible value at $n=N/2$, and then decreases until $n=N$. All sensitivities are positive and different from zero. The advantages of this second strategy are that the sensitivities for mode numbers $n \lesssim N/2$ are about two times larger than in the first strategy. Also, the spot diameter is about two times larger than in the first strategy (larger spot diameters are usually easier to produce). The main disadvantage of the second strategy is that the sensitivities for mode numbers $n \gtrsim N/2$ are lower than in the first strategy. This becomes critical if the bandwidth of the detection electronics is limited to low frequencies. (3) If it is acceptable that the detection sensitivities for some modes are negative, the spot diameter and position could be chosen such that the sensitivity of the $(N+1)^{\text{th}}$ mode coincides with the second zero of $\Omega_{0.424}(u)$: $w/L_{\text{eff}} \cong 3.94/(N+1/2)$ and $\varepsilon \cong 0.424$. The advantages of this third strategy are even more pronounced than those of the second strategy; the sensitivities for small normal mode numbers are about four times larger than in the first strategy, and the spot diameter is also about four times larger. Mixed positive and negative sensitivities, however, might complicate further processing.

In many practical cases, however, it is not easily possible to adjust the diameter of the focused spot. Therefore, we now also discuss a strategy for optimizing the detection sensitivities for multiple normal modes for a fixed spot diameter. In the case that the spot diameter is small enough so that one of the strategies above can be applied, then it is best to place the spot close to the tip according to Eq. (14) with $\varepsilon \cong 0.424$ [we note that for very small spot diameters, $\approx$25% additional sensitivity is achieved when positioning the spot slightly closer to the base ($\varepsilon \cong 0.8$)]. In those strategies, however, near-zero sensitivities will result for mode numbers $n \geqslant 3.94 L_{\text{eff}}/w + 1/2$. So if the spot diameter is too large, then a fourth strategy should be applied, in which the spot is positioned exactly at the tip ($\varepsilon=0$, i.e., $p_b = L_{\text{eff}}$). For this spot position, relatively large sensitivities occur for large mode numbers [see Fig. 4(b)]. The maximum detection sensitivity in this case is obtained for mode number $n \cong 1.45 L_{\text{eff}}/w + 1/2 [\Omega_0(1.45) \cong 0.746]$. For further increasing mode numbers, the sensitivity decreases and drops below 10% of the value at the maximum for $n \leqslant 8.42 L_{\text{eff}}/w + 1/2$. The disadvantage of this fourth strategy is that small mode numbers are detected with a reduced sensitivity ($\approx$32% of the sensitivity when $\varepsilon \cong 0.424$). Note that no gain in sensitivity is obtained for even smaller ε.

Two examples using these results will now be given. (1) Suppose that all normal modes up to mode number $N=20$ of a cantilever with $L_{\text{eff}}=200\ \mu$m need to be detected simultaneously with positive detection sensitivity. The optimum spot diameter could be chosen in line with either the first or the second strategy. When using the first strategy, $w \cong 0.814/(20-1/2)(200\ \mu\text{m}) \cong 8.3\ \mu$m, and the detection sensitivity increases monotonically from the 1st to the 20th mode [case $N=20$ in Fig. 4(a)]. When using the second strategy, the optimum spot diameter is $w \cong 1.75/(20+1/2) \times (200\ \mu\text{m}) \cong 17.1\ \mu$m, and the sensitivity initially monotonically increases with increasing mode number, peaks at mode number $n \approx 10$, and then monotonically decreases until mode number $n=20$, while the sensitivity is always positive and nonzero. In both strategies, $\varepsilon=0.424$, i.e., the spot is positioned on the cantilever such that the distance of the spot center to the tip is 0.424$\times$ the spot diameter. Practically, this spot position could be found by moving the spot from the base toward the tip until 4.5% of the total power of the incident beam is spilled over the edge at the tip. (2) Consider an AFM for small cantilevers[17,34] with a focused spot size of $w=4.0\ \mu$m, and a small cantilever[35,36] with an effective length $L_{\text{eff}}=12\ \mu$m [case $N=3$ in Fig. 4(a)]. When positioning the spot using $\varepsilon=0.424$ (strategies 1–3), the largest detection sensitivity is achieved already for the third mode. Positive, nonzero sensitivities are obtained until the fifth mode, fairly large negative sensitivities are obtained at around the eighth mode, and no modes are detected with a significant sensitivity above the 12th mode. However, when positioning the spot at exactly the tip ($\varepsilon=0$ or $p_b = L_{\text{eff}}$ i.e., allowing half of the incident-beam power to be spilled over the edge at the tip) (strategy 4), the largest detection sensitivity is obtained for mode number $n \cong 1.45(12\ \mu\text{m})/(4.0\ \mu\text{m}) + 1/2 \cong 5$, and the sensitivity stays above 10% of that value for mode numbers $n \leqslant 8.42(12\ \mu\text{m})/(4.0\ \mu\text{m}) + 1/2 \cong 26$. So more than 2$\times$ as many normal modes can be detected when positioning the spot center exactly at the tip, as compared to the case when positioning the spot center further towards the base according to $\varepsilon=0.424$.

IV. CONCLUSION

We have presented a detailed theoretical investigation of the sensitivity with which normal vibration modes of AFM cantilevers are detected using the optical beam deflection method. Arbitrary angular orientations of cantilever, incident beam, and scanner, respectively, were considered. Global and locally restricted optimizations of the sensitivity were performed individually for each mode by varying the diameter and position of the focused spot. Interestingly, optimum sensitivity for higher-order modes is achieved when the spot is positioned close to the base of the cantilever and not close to the tip as might have been expected. The corresponding spot diameter is 59% of the mode wavelength. Normal modes number 2 and higher can be detected with a $\approx$2$\times$ larger sensitivity than mode number 1, suggesting that higher-order modes can be advantageous for imaging and spectroscopy applications. For the simultaneous detection of multiple normal modes, however, it is generally of advantage to position the spot close to the tip. We constructed a universal sensitivity function from which the sensitivities for all modes can be

extracted, and discussed different optimization strategies for the simultaneous detection of multiple normal modes. For small spot diameters, the strategy is to position the spot on the cantilever such that the distance from the spot center to the tip is $\approx 0.424\times$ the spot diameter. For large spot diameters, the strategy is to position the spot center exactly at the tip of the cantilever.

ACKNOWLEDGMENTS

We thank Boris Anczykowski for a critical reading of the manuscript. This work was supported by the Gemeinnützige Hertie-Stiftung/Stifterverband für die Deutsche Wissenschaft.

[1]G. Binnig, C. F. Quate, and C. Gerber, Phys. Rev. Lett. **56**, 930 (1986).
[2]Q. Zhong, D. Inniss, K. Kjoller, and V. B. Elings, Surf. Sci. **290**, L688 (1993).
[3]P. K. Hansma, *et al.*, Appl. Phys. Lett. **64**, 1738 (1994).
[4]T. R. Albrecht, P. Grütter, D. Horne, and D. Rugar, J. Appl. Phys. **69**, 668 (1991).
[5]F. J. Giessibl, Science **267**, 68 (1995).
[6]Y. Sugawara, M. Ohta, H. Ueyama, and S. Morita, Science **270**, 1646 (1995).
[7]B. Cappella and G. Dietler, Surf. Sci. Rep. **34**, 1 (1999).
[8]H. Clausen-Schaumann, M. Seitz, R. Krautbauer, and H. E. Gaub, Curr. Opin. Chem. Biol. **4**, 524 (2000).
[9]Y. Z. Liu, S. H. Leuba, and S. M. Lindsay, Langmuir **15**, 8547 (1999).
[10]U. Dürig, Appl. Phys. Lett. **75**, 433 (1999).
[11]H. Hölscher, A. Schwarz, W. Allers, U. D. Schwarz, and R. Wiesendanger, Phys. Rev. B **61**, 12678 (2000).
[12]S. Morita, R. Wiesendanger, and E. Meyer, *Noncontact Atomic Force Microscopy* (Springer, Berlin, 2002).
[13]S. C. Minne, S. R. Manalis, A. Atalar, and C. F. Quate, Appl. Phys. Lett. **68**, 1427 (1996).
[14]U. Rabe and W. Arnold, Appl. Phys. Lett. **64**, 1493 (1994).
[15]K. Yamanaka, H. Ogiso, and O. Kolosov, Appl. Phys. Lett. **64**, 178 (1994).
[16]U. Rabe, K. Janser, and W. Arnold, Rev. Sci. Instrum. **67**, 3281 (1996).
[17]T. E. Schäffer, J. P. Cleveland, F. Ohnesorge, D. A. Walters, and P. K. Hansma, J. Appl. Phys. **80**, 3622 (1996).
[18]R. W. Stark, T. Drobek, and W. M. Heckl, Appl. Phys. Lett. **74**, 3296 (1999).
[19]R. Hillenbrand, M. Stark, and R. Guckenberger, Appl. Phys. Lett. **76**, 3478 (2000).
[20]R. W. Stark and W. M. Heckl, Surf. Sci. **457**, 219 (2000).
[21]M. Stark, R. W. Stark, W. M. Heckl, and R. Guckenberger, Proc. Natl. Acad. Sci. U.S.A. **99**, 8473 (2002).
[22]T. R. Rodríguez and R. García, Appl. Phys. Lett. **84**, 449 (2004).
[23]G. Meyer and N. M. Amer, Appl. Phys. Lett. **53**, 1045 (1988).
[24]S. Alexander, L. Hellemans, O. Marti, J. Schneir, V. Elings, P. K. Hansma, M. Longmire, and J. Gurley, J. Appl. Phys. **65**, 164 (1989).
[25]T. E. Schäffer and P. K. Hansma, J. Appl. Phys. **84**, 4661 (1998).
[26]T. E. Schäffer, J. Appl. Phys. **91**, 4739 (2002).
[27]T. E. Schäffer, Nanotechnology **16**, 664 (2005).
[28]R. Proksch, T. E. Schäffer, J. P. Cleveland, R. C. Callahan, and M. B. Viani, Nanotechnology **15**, 1344 (2004).
[29]R. W. Stark, Rev. Sci. Instrum. **75** 5053 (2004).
[30]S. Timoshenko, D. H. Young, and W. Weaver, *Vibration Problems in Engineering* (Wiley, New York, 1974).
[31]M. G. L. Gustafsson and J. Clarke, J. Appl. Phys. **76**, 172 (1994).
[32]C. A. J. Putman, B. G. De Grooth, N. F. Van Hulst, and J. Greve, J. Appl. Phys. **72**, 6 (1992).
[33]H. J. Butt and M. Jaschke, Nanotechnology **6**, 1 (1995).
[34]T. E. Schäffer, M. Viani, D. A. Walters, B. Drake, E. K. Runge, J. P. Cleveland, M. A. Wendman, and P. K. Hansma, Proc. SPIE **3009**, 48 (1997).
[35]D. A. Walters, J. P. Cleveland, N. H. Thomson, P. K. Hansma, M. A. Wendman, G. Gurley, and V. Elings, Rev. Sci. Instrum. **67**, 3583 (1996).
[36]M. B. Viani, T. E. Schäffer, A. Chand, M. Rief, H. E. Gaub, and P. K. Hansma, J. Appl. Phys. **86**, 2258 (1999).